Solar zenith angle dependencies of F1-layer, NmF2 negative disturbance, and G-condition occurrence probabilities

V. V. Lobzin, A. V. Pavlov

▶ **To cite this version:**

V. V. Lobzin, A. V. Pavlov. Solar zenith angle dependencies of F1-layer, NmF2 negative disturbance, and G-condition occurrence probabilities. Annales Geophysicae, 2002, 20 (11), pp.1821-1836. hal-00317387

HAL Id: hal-00317387
https://hal.science/hal-00317387

Submitted on 1 Jan 2002

HAL is a multi-disciplinary open access archive for the deposit and dissemination of scientific research documents, whether they are published or not. The documents may come from teaching and research institutions in France or abroad, or from public or private research centers.

L'archive ouverte pluridisciplinaire **HAL**, est destinée au dépôt et à la diffusion de documents scientifiques de niveau recherche, publiés ou non, émanant des établissements d'enseignement et de recherche français ou étrangers, des laboratoires publics ou privés.

Annales Geophysicae (2002) 20: 1821–1836 © European Geosciences Union 2002

Annales Geophysicae

Solar zenith angle dependencies of F1-layer, *Nm*F2 negative disturbance, and G-condition occurrence probabilities

V. V. Lobzin and A. V. Pavlov

Institute of Terrestrial Magnetism, Ionosphere, and Radio-Wave Propagation, Russian Academy of Sciences (IZMIRAN), Troitsk, Moscow Region, 142190, Russia

Received: 10 January 2002 – Revised: 5 April 2002 – Accepted: 28 May 2002

Abstract. Experimental data acquired by the Ionospheric Digital Database of the National Geophysical Data Center, Boulder, Colorado, from 1957 to 1990, are used to study the dependence of the G condition, F1-layer, and *Nm*F2 negative disturbance occurrence probabilities on the solar zenith angle during summer, winter, spring, and autumn months in latitude range 1 (between $-10°$ and $+10°$ of the geomagnetic latitude, Φ), in latitude range 2 ($10° < |\Phi| \leq 30°$), in latitude range 3 ($30° < |\varphi| \leq 45°, 30° < |\Phi| \leq 45°$), in latitude range 4 ($45° < |\varphi| \leq 60°, 45° < |\Phi| \leq 60°$), and in latitude range 5 ($60° < |\Phi| \leq 90°$), where φ is the geographic latitude. Our calculations show that the G condition is more likely to occur during the first half of a day than during the second half of a day, at all latitudes during all seasons for the same value of the solar zenith angle. The F1-layer occurrence probability is larger in the first half of a day in comparison with that in the second half of a day for the same value of the solar zenith angle in latitude range 1 for all seasons, while the F1-layer occurrence probability is approximately the same for the same solar zenith angle before and after noon in latitude ranges 4 and 5. The F1-layer and G condition are more commonly formed near midday than close to post sunrise or pre-sunset. The chance that the daytime F1-layer and G condition will be formed is greater in summer than in winter at the given solar zenith angle in latitude ranges 2–5, while the F1-layer occurrence probability is greater in winter than in summer for any solar zenith angle in latitude range 1. The calculated occurrence probability of the *Nm*F2 weak negative disturbances reaches its maximum and minimum values during daytime and night-time conditions, respectively, and the average night-time value of this probability is less than that by day for all seasons in all studied latitude regions. It is shown that the *Nm*F2 normal, strong, and very strong negative disturbances are more frequent on average at night than by day in latitude ranges 1 and 2 for all seasons, reaching their maximum and minimum occurrence probability values at night and by day, respectively. This conclusion is also correct for all other studied latitude regions during winter months, except for the *Nm*F2 normal and strong negative disturbances in latitude range 5. A difference in the dependence of the strong and very strong *Nm*F2 negative disturbance percentage occurrences on the solar zenith angle is found between latitude ranges 1 and 2. Our results provide evidence that the daytime dependence of the G condition occurrence probability on the solar zenith angle is determined mainly by the dependence of the F1-layer occurrence probability on the solar zenith angle in the studied latitude regions for winter months, in latitude range 2 for all seasons, and in latitude ranges 4 and 5 for spring, summer, and autumn months. The solar zenith angle trend in the probability of the G condition occurrence in latitude range 3 arises in the main from the solar zenith angle trend in the F1-layer occurrence probability. The solar zenith angle trend in the probabilities of strong and very strong *Nm*F2 negative disturbances counteracts the identified solar zenith angle trend in the probability of the G condition occurrence.

Key words. Ionosphere (ionospheric disturbances, ionosphere-atmosphere interactions, ion chemistry and composition)

1 Introduction

The Ionospheric Digital Database of the National Geophysical Data Center, Boulder, Colorado, provides the routine sounding ground-based station measurements of the critical frequencies and virtual heights of different ionospheric layers, and, in particular, the critical frequencies *fo*f1 and *fo*f2 of F1- and F2-layers that are analyzed in this study. The values of the peak densities, *Nm*F1 and *Nm*F2, of the F1- and F2-layers are related to the critical frequencies *fo*f2 and *fo*f1 as $NmF2 = 1.24 \times 10^{10}\ foF2^2$ and $NmF1 = 1.24 \times 10^{10}\ foF1^2$, where the unit of *Nm*F2 and *Nm*F1 is m^{-3}, the unit of *fo*f2 and *fo*f1 is MHz (URSI handbook of ionogram interpretation and reduction, 1978). The Ionospheric Digital Database is

Correspondence to: A. V. Pavlov (pavlov@izmiran.rssi.ru)

formed using the URSI standard rules (URSI handbook of ionogram interpretation and reduction, 1978). In addition to numerical values of ionospheric parameters, the qualifying and descriptive letters A–Z are used in this database. The descriptive letter G means that a measurement is influenced by, or impossible because, the ionization density of the layer is too small to enable it to be made accurately, and this case is described as a G condition in the F-region of the ionosphere when $fo2 \leq fo1$ (URSI handbook of ionogram interpretation and reduction, 1978). If the layer is not seen from ionograms due to other reasons, then other letters are used. The G condition arises in the ionosphere when the critical frequency of the F2-layer drops below that of the F1-layer, i.e. when the peak density, *Nm*F1, of the F1-layer, which is composed mostly of the molecular ions NO^+ and $O2^+$, is larger than that of the F2-layer, which is dominated by O^+ ions (King, 1962). As a result, a very low main peak altitude value (below 200 km) is observed in ionograms, so that no information is obtainable above this height from ground-based ionozonde data. As far as the authors know, the first altitude distribution of the electron density during a G condition was deduced by Norton (1969) from ionograms recorded by the Alouette I satellite ionozonde and the St. John's ground-based ionozonde during the severe negative ionospheric storm on 18 April 1965.

The physics of the G condition phenomenon has been studied by Buonsanto (1990) using ionosonde data from two mid-latitude stations, by Oliver (1990), using Millstone Hill incoherent scatter radar data, and by Fukao et al. (1991) using data from the middle and upper atmosphere radar in Japan. Pavlov and Buonsanto (1998), Pavlov (1998), Pavlov et al. (1999), Schlesier and Buonsanto (1999), and Pavlov and Foster (2001) studied the G condition formation for quiet and disturbed mid-latitude ionosphere during periods of low, moderate, and high solar activity, using the Millstone Hill incoherent scatter radar data. Model results also show that O^+ can become a minor ion in the F-region, creating a G condition during disturbed conditions at high latitudes (Banks et al., 1974; Schunk et al., 1975), and observations at EISCAT confirm this conclusion (e.g. Häggström and Collis, 1990). These papers provide evidence that changes in [O], $[N_2]$, $[O_2]$, and the plasma drift velocity, the effect of the perpendicular (with respect to the geomagnetic field) component of the electric field on the electron density (through changes in the rate coefficients of chemical reactions of ions), and the effects of vibrationally excited N_2 and O_2 on the electron density are important factors that control the G condition formation in the ionosphere. The study of the G condition formation in the ionosphere above Millstone Hill during the severe geomagnetic storm of 15–16 July 2000, provided a weighty argument for the inclusion of the effects of vibrationally excited N_2 and O_2 on the electron density and temperature in ionospheric models (Pavlov and Foster, 2001).

During *Nm*F2 disturbances, which are believed to be caused by geomagnetic storms and substorms, the value of *Nm*F2 can either increase or decrease in comparison with a geomagnetically quiet *Nm*F2, and these changes are denoted as positive and negative disturbances (Prölss, 1995; Buonsanto, 1999). A decrease in *Nm*F2 during a *Nm*F2 negative disturbance leads to an increase in the G condition occurrence probability if the F1-layer exists. On the other hand, the G condition cannot exist in the ionosphere if there is no F1-layer. The preceding work by Lobzin and Pavlov (2002) summarizes papers addressing the measurements and the physics of the F1-layer, *Nm*F2 negative disturbance, and G condition, and gives for the first time the detailed dependencies of the probabilities of the F1-layer, *Nm*F2 negative disturbance, and G condition occurrences on a daily solar activity index, F10.7, a 3-h geomagnetic index, K_p, a number of a given day in a year, and a geomagnetic latitude. The aim of this paper is to carry out a statistical study of solar zenith angle dependencies of *Nm*F1, *Nm*F2 negative disturbance, and G condition occurrence probabilities using the Digital Database *fo*1 and *fo*2 measurements from 1957 to 1990.

Some features of the solar zenith angle dependencies of *Nm*F1, *Nm*F2 negative disturbance, and G condition occurrence frequencies have been known for a long time. Ratcliffe (1956, 1972), Yonezawa et al. (1959) concluded that the F1-layer is less liable to appear for larger values of the solar zenith angle. Du Charme and Petrie (1973) derived an expression to predict *fo*1, assuming limits for the presence of the F1-layer as a function of the solar zenith angle and of solar activity. Scotto et al. (1997) tested the Du Charme and Petrie (1973) formula adopted in the International Reference Ionosphere (IRI) model, taking into account alternative solutions for the particular restrictions imposed by the IRI for high values of solar zenith angle. New probability functions to predict the occurrence of the F1-layer have been proposed by Scotto et al. (1997, 1998) to replace the Du Charme and Petrie (1973) formula.

A negative F2 ionospheric storm onset at middle latitudes is most frequently observed in the morning time sector and very rarely in the noon, afternoon, and night-time sectors (Prölss, 1995; Buonsanto, 1999). Wrenn et al. (1987) discriminated geomagnetic activity levels as very quiet, quiet, normal, disturbed, and very disturbed conditions. The negative ionospheric storm effect in *Nm*F2 during normal, disturbed, and very disturbed conditions is centered at night for very disturbed conditions and during morning hours for normal and disturbed conditions if the ionozonde *fo*2 measurements from the Argentine Islands ionozonde station are used (Wrenn et al., 1987). The comparison between the summer *fo*2 measurements of the Argentine Islands and Port Stanley ionozonde stations leads to the conclusion that the maximum *fo*2 depression moves from the night-time sector to the morning sector if the latitude of the station is changed from middle to more low latitudes (Wrenn et al., 1987). It is found by Ratcliffe (1972) that the G condition is more commonly formed near midday than during several hours after sunrise or before sunset. However, the results of Ratcliffe (1972) are not formulated in a mathematical form to be used in calculations.

Previous investigations are based on the limited ionozonde

data set from some stations and on theoretical analysis of the main physical processes that form electron density altitude profiles. As a result, except for the Scotto et al. (1997, 1998) formulas for the F1-layer probability function, there are no published solar zenith angle dependencies of *Nm*F1, *Nm*F2 negative disturbance, and G condition occurrence probabilities. The main purpose of this work is to calculate for the first time these probabilities for low, middle, and high latitudes in summer, in winter, and during the spring and autumn months, to provide some quantitative measure of these probability variations. In our analysis we study for the first time a possible relationship between the solar zenith angle probability dependence of the G condition occurrence with the solar zenith angle probability dependencies of *Nm*F2 negative disturbance and F1-layer occurrences.

2 Formation of the F1- and F2-layers in the ionosphere

Solar zenith angle dependencies of *Nm*F1 and *Nm*F2 negative disturbance and G condition occurrence probabilities, which are studied in our work, are determined by physical processes that form the F-region of the ionosphere. The F-region is located in the altitude range above 140–160 km. Within the F-region are the F1- and F2-layers, with the peak altitudes $hm\mathrm{F1} < 190 - 200$ km and $hm\mathrm{F2} > 200 - 210$ km, respectively. The major F1- and F2-layer ions are $O^+(^4S)$, O_2^+, and NO^+. The main physical processes that form the F1 and F2-layers in the ionosphere by a balance between production, chemical loss, and transport of electrons and ions are described in many review articles, books, and papers (e.g. Ratcliffe, 1972; Rishbeth and Garriot, 1969; Brunelli and Namgaladze, 1988; Rees, 1989; Fejer, 1997; Rishbeth and Muller-Wodarg, 1999; Rishbeth, 2000; Rishbeth et al., 2000; Abdu, 2001; Lobzin and Pavlov, 2002; Pavlov and Foster, 2001). Following these studies, it is usually supposed that the value of *Nm*F2 is approximately directly proportional to the [O]/L ratio at $\widehat{h}m\mathrm{F2}$ during daytime conditions, where L is the loss rate of $O^+(^4S)$ ions in the reactions of $O^+(^4S)$ with unexcited $N_2(v = 0)$ and $O_2(v = 0)$ and vibrationally excited $N_2(v)$ and $O_2(v)$ molecules at vibrational levels, $v > 0$. Thus, the depletion in [O] and the increase in $[N_2]$ and $[O_2]$ can lead to a negative phase in *Nm*F2. The increase in the rate coefficients for reactions between $O^+(^4S)$ ions and $N_2(v \geq 0)$ and $O_2(v \geq 0)$, due to changes in neutral and ion temperatures and due to the increase in vibrational temperatures of N_2 and O_2 would also produce negative storm effects in *Nm*F2. These assumptions are used in our study in discussions of *Nm*F2 variation sources and to understand reasons for solar zenith angle dependencies of *Nm*F2 negative disturbance and G condition occurrence probabilities.

To illustrate the basic physics involved and to study the physical reasons for *Nm*F2 negative disturbance occurrence probability nighttime variations, it is useful to use the analytical approximation of the nighttime mid-latitude *Nm*F2 given by Krinberg and Tashchilin (1982, 1984) as

$$Nm\mathrm{F2}(t) \approx Nm\mathrm{F2}(t_0) \exp\left[-(t - t_0)L(t)\right] + 3F_\infty(t)T_n(t)\nu_{in}(t)/\left(g\left[T_i(t) + T_e(t)\right]\right), \quad (1)$$

where t is a local time, $Nm\mathrm{F2}(t_0)$ is the ionospheric electron density for the local time t_0 corresponding to dusk, T_n is the exospheric neutral temperature, T_i and T_e are ion and electron temperatures, g is the acceleration due to gravity, ν_{in} is the $O^+ - O$ collision frequency, F_∞ is the value of plasma ion flux flowing from the plasmasphere into the ionosphere, the values of L, T_i, T_e, g, and ν_{in} are chosen at the F2 peak altitude.

One can see from Eq. (1) that the nighttime F2-region electron density consists of two parts. The first term describes the role of the daytime ionization in the maintenance of the nighttime ionosphere. In this case the F-region would decay with the characteristic time $\sim L^{-1}$ (about several hours). Since the loss rate of $O^+(^4S)$ ions is proportional to $[N_2]$ and $[O_2]$, an increase or decrease in $[N_2]$ and $[O_2]$ at $\widehat{h}m\mathrm{F2}$ altitudes leads to a decrease or an increase in *Nm*F2, respectively. The nocturnal F-region is also maintained by a downward flow of ionization from the plasmasphere, described by the second term in Eq. (1). In winter, and possibly in spring and in autumn, when the night is long enough, the role of the second term in Eq. (1) increases before sunrise, and this term can determine the mid-latitude value of *Nm*F2.

The role of the ion transport is less than the role of the chemical reactions of ions with electrons and neutral components of the upper atmosphere at the F1-layer altitudes, and the production and loss rates of electrons and ions that determine the F1-layer formation. To study the formation of the F1-layer, Ratcliffe (1972) assumed that the main source of NO^+ ions is the chemical reaction of O^+ with N_2, and there are only NO^+ and O^+ ions. Ratcliffe (1972) found that the peak of the F1-layer exists in the ionosphere if the peak altitude, h_0, of the total production rate of thermal electrons is less than an altitude, h_t. The value of h_t is determined from the condition of $K\ [N_2] = \alpha[e]$, where K is the rate coefficient for the reaction of O^+ ions with N_2, and α is the rate coefficient of the dissociative recombination of NO^+ ions. Ratcliffe (1972) concluded that the value of $h_t - h_0$ is decreased with the solar activity level increase, and the value of $h_t - h_0$ has a maximum value close to midday. As a result, the F1 peak is more clearly in evidence at solar minimum than at solar maximum, and the F1 peak is more commonly formed near midday and in summer (Ratcliffe, 1972).

Yonezawa et al. (1959) carried out another simple consideration for the F1-layer to appear as a distinct layer. In addition to the equality of α and the rate coefficient of the dissociative recombination of O_2^+ ions, the height gradient of the atmospheric neutral components, the rate coefficients of O^+ ions with N_2 and O_2, and the value of α were assumed to be constants by Yonezawa et al. (1959), to obtain the condition of appearance of the F1-layer as

$$(\alpha Q_0)^{0.5} < 0.089 L(h = h_0)(\cos\chi)^{1.65}, \quad (2)$$

where Q_0 is the maximum production rate of electron-ion pairs for the Sun by photoionization of atomic oxygen at an altitude, $h = h_0$.

Using Eq. (2), Yonezawa et al. (1959) concluded that the F1-layer is more liable to appear during periods of low solar activity than during periods of high solar activity, and during the day near noon than near sunrise or sunset. It follows from Eq. (2) that the *Nm*F1 occurrence probability approaches 100% if Eq. (2) is valid and 0% if Eq. (2) is not realized in the ionosphere.

The ionosphere at low latitudes is very sensitive to electric fields. The daytime low latitude electric field that is directed eastward causes the ionosphere to be lifted to high altitudes along magnetic field lines, where there is a very rapid diffusion of electrons and ions, and gravity pull the electrons and ions downward and poleward on either side of the magnetic equator, so that a low latitude trough develops over the equator, with the F2-layer density maximum to the north and south (Rishbeth, 2000; Abdu, 2001). This F2-layer structure is usually called the equatorial or Appleton anomaly. If the daytime eastward electric field is strengthened or weakened during geomagnetic storms and substorms, the F2-layer density maximum move further poleward or equatorward, and the ionospheric density over the equator is reduced or increased, respectively. It is remarkable that the upward drift by day is balanced by a downward drift at night, and *hm*F2 is lower at night than by day at low latitudes, while the middle latitude *hm*F2 is higher at night than by day. According to Sterling et al. (1972), the low-latitude F1-layer is caused by the electromagnetic drift, rather than by an effect of F1-layer photochemistry.

3 Data and method of data analysis

Ionograms produced by ionozondes are records that show variations of the virtual height of radio wave reflection from the ionosphere as a function of the radio frequency, $h'(f)$, within the frequency band range 1 MHz–20 MHz that is normally used (URSI handbook of ionogram interpretation and reduction, 1978). The radio wave that is reflected from the ionosphere level of ionization is split into two waves of different polarization in the Earth's magnetic field, thereby leading to two sorts of observed $h'(f)$ curves. These waves are called the ordinary wave (o-mode) and the extraordinary wave (x-mode). There are also z-mode traces on some ionograms generated by radio waves which have been propagated along the magnetic field lines. The mode traces can be identified by the frequency separation and by other indications presented in the URSI handbook of ionogram interpretation and reduction (1978). A simple approach is used to find peak electron densities of the ionosphere from observations of $h'(f)$ curves. When the level of the peak electron density in the layer is reached, the value of $h'(f)$ becomes effectively infinite ($\frac{df}{dh'} \to 0$). The frequency at which this occurs is determined as the critical frequency of the ionospheric layer.

Our analysis is based on 34 years of hourly *fo*F2 and *fo*F1 data from 1957 to 1990 from stations available on the Ionospheric Digital Database of the National Geophysical Data Center, Boulder, Colorado. At the chosen ionozonde station, the solar zenith angle, χ, is a function of a local time, a geographic latitude, and a number, n_d, of a given day in a year. Therefore, a multiple-parameter statistics is needed to study the solar zenith angle dependencies of *Nm*F2 negative disturbance, *Nm*F1, and G condition occurrences. We do not analyze the ionozonde measurements of *fo*F2 and *fo*F1 in the Northern Hemisphere and the Southern Hemisphere separately, but carry out our statistical analysis of solar zenith angle dependencies of *Nm*F1, *Nm*F2 negative disturbance, and G condition occurrences separately in summer (June, July, and August in the Northern Hemisphere, and December, January, and February in the Southern Hemisphere), in winter (December, January, and February in the Northern Hemisphere, and June, July, and August in the Southern Hemisphere), and during spring and autumn months (March, April, May, September, October, and November in both hemispheres).

As we have pointed out, the solar zenith angle is a function of geographic latitude, φ. Therefore, to study the solar zenith angle dependencies of *Nm*F2 negative disturbance, F1-layer, and G condition occurrences, the geographic latitude range has to be taken so that this range is minimized, while the number of measurements remains large enough to carry out this statistical study. On the other hand, there are significant differences in physical processes that determine *Nm*F2 negative disturbance, *Nm*F1, and G condition occurrences at low, middle, and high geomagnetic latitudes, Φ (e.g. Ratcliffe, 1972; Rishbeth and Garriot, 1969; Brunelli and Namgaladze, 1988; Rees, 1989; Fejer, 1997; Rishbeth and Muller-Wodarg, 1999; Rishbeth et al., 2000; Lobzin and Pavlov, 2002), and these differences can lead to differences in the solar zenith angle dependencies of the studied events. Therefore, we split the ionozonde *fo*F2 and *fo*F1 data set used into five parts. A geomagnetic equatorial region ($-10° \le \Phi \le 10°$), where an equatorial daytime *Nm*F2 trough is developed, is defined in our study as a latitude range 1. A latitude range 2 is a low-latitude region ($10° < |\Phi| \le 30°$) where daytime *Nm*F2 crests in comparison when equatorial daytime *Nm*F2 are observed. Latitude ranges 3 and 4 are mid-latitude regions. A latitude range 3 includes both $30° < |\varphi| \le 45°$ and $30° < |\Phi| \le 45°$. A latitude range 4 includes both $45° < |\varphi| \le 60°$ and $45° < |\Phi| \le 60°$. It is clear from the definition of these mid-latitude ranges that latitude ranges 3 and 4 are not overlapping.

The main ionization trough, the ionization hole in the polar cap around local dawn, the tongue of ionization, and the aurorally produced ionization electron density peak in the vicinity of the auroral oval are a natural consequence of the difference and competition between the various chemical and transport processes known to be operating in the high-latitude F-region ionosphere (for more details, see, e.g. Rees, 1989; Buonsanto, 1999). The latitude and longitude boundaries of these regions show marked variations. As a result, only average solar zenith angle dependencies of *Nm*F1, *Nm*F2 negative disturbance, and G condition probability functions in a latitude range 5 ($60° < |\Phi| \le 90°$) are calculated in this paper. To discriminate between the

Table 1. Average values of F1-layer and G condition percentage occurrences in latitude ranges 1–5 during the winter, summer, and spring and autumn months for the first (first number) and second (second number) half of the day for $\chi \leq 90°$

		Latitude range 1	Latitude range 2	Latitude range 3	Latitude range 4	Latitude range 5
F1 layer	Winter	14.1, 11.2	18.2, 18.4	19.5, 18.5	13.4, 12.9	11.6, 13.4
	Summer	12.2, 9.5	27.0, 23.9	38.6, 35.9	48.1, 41.4	49.8, 46.7
	Spring, autumn	9.1, 6.5	18.4, 16.8	31.5, 26.8	36.9, 32.2	43.8, 44.1
G condition	Winter	–	–	0.1, 0.1	0.2, 0.1	0.8, 0.6
	Summer	–	0.3, 0.1	0.9, 0.5	1.7, 0.5	3.8, 2.0
	Spring, autumn	–	0.05, 0.03	0.6, 0.4	1.4, 0.6	2.2, 2.0

morning and evening solar zenith angle dependencies of the studied events, we split the range of $0° \leq \chi \leq 180°$ into twelve intervals of the same length, $\Delta\chi$, both from 00:00 LT to 12:00 LT, and from 12:00 LT to 24:00 LT at each ionozonde station.

We consider the measured *fo*f1 and *fo*f2 within the above-determined local time, latitude, and month range, and determine the probability, $\Psi_G(\chi)$, or $\Psi_{F1}(\chi)$, of the G condition or F1-layer occurrence as a ratio of the number of G condition or F1-layer observations for zenith angles within the $\Delta\chi$ interval to a total number of measurements for the same $\Delta\chi$ and within the given local time, latitude, and month range.

The electron density can either decrease or increase during geomagnetically disturbed conditions, and these electron density changes are denoted as negative and positive ionospheric disturbances, respectively. To test the effects of geomagnetic activity, we use two different K_p labels: "disturbed", for which we take $K_p > 3$ and use the peak density, *Nm*F2(d), and critical frequency, *fo*f2(d), of the F2-layer observed during the time periods with $K_p > 3$, and "quiet", for which we take $K_p \leq 3$. The determination of the quiet peak density, *Nm*F2(q), and critical frequency, *fo*f2(q), of the F2-layer, is crucial for studies of negative and positive ionospheric disturbances.

Perturbations in the neutral composition, temperature, and wind at one altitude are rapidly transmitted to higher and lower altitudes. However, it takes time to relax back to an initial state of the thermosphere, and this thermosphere relaxation determines the time for the disturbed ionosphere to relax back to the quiet state. It means that not every *fo*f2 observed during the day with $K_p \leq 3$ can be considered as *fo*f2(q). The characteristic time of the neutral composition recovery after a storm impulse event ranges from 7 to 12 h on average (Hedin, 1987), while it may need up to several days for all altitudes down to 120 km in the atmosphere to recover completely back to the undisturbed state of the atmosphere (Richmond and Lu, 2000). As a result of this thermosphere recovery, a day with $K_p \leq 3$ from 00:00 UT to 24:00 UT cannot be considered a quiet day if the previous day was a day with $K_p > 3$ from 00:00 UT to 24:00 UT. We determine the quiet reference day with *fo*f2(q) as a day with $K_p \leq 3$ from 00:00 UT to 24:00 UT if the previous day was a day with $K_p \leq 3$ from 00:00 UT to 24:00 UT. Furthermore, we only use the quiet day with the uninterrupted *fo*f2 measurements from 00:00 UT to 24:00 UT, and the comparison between *fo*f2(d) and *fo*f2(q) measured at the chosen station is carried out if the time difference between *fo*f2(d) and *fo*f2(q) measurements is less than or equal to 30 days. We use the nearest quiet day to the studied disturbed time period, and determine the relative deviation, δ, of *fo*f2 observed at the given station from *fo*f2(q) as

$$\delta = foF2(d)/foF2(q) - 1 = (NmF2(d)/NmF2(q))^{1/2} - 1. \quad (3)$$

Negative and positive values of δ correspond to negative and positive disturbances in *Nm*F2, respectively. We study the dependence of the probabilities of the negative disturbance occurrences in *Nm*F2 on χ. Following the preceding work by Lobzin and Pavlov (2002), we give negative *fo*f2 disturbances the labels "weak" ($-0.1 < \delta < 0$ or $0.81 < NmF2(d)/NmF2(q) < 1$), "normal" ($-0.3 < \delta \leq -0.1$ or $0.49 < NmF2(d)/NmF2(q) \leq 0.81$), "strong" ($0.5 < \delta \leq -0.3$ or $0.25 < NmF2(d)/NmF2(q) \leq 0.49$), and "very strong" ($\delta \leq -0.5$ or $NmF2(d)/NmF2(q) \leq 0.25$), and confine our attention to relationships between them and the G condition or F1-layer occurrences.

Similar to the $\Psi_G(\chi)$ and $\Psi_{F1}(\chi)$ determinations, we analyze the measured *fo*f1 and *fo*f2 within each above-determined latitude, month and local time range. We determine the probability, $\Psi_{\delta 1 \leq \delta \leq \delta 0}(\chi)$, of the *Nm*F2 negative disturbance occurrence as a ratio of a number of *Nm*F2 negative disturbance observations within the $\delta 1 \leq \delta \leq \delta 0$ range for zenith angles within the $\Delta\chi$ interval to a total number of studied *Nm*F2 negative and positive disturbance observations for the same $\Delta\chi$, within the given latitude, month, and local time range.

4 Results and discussion

4.1 F1-layer and G condition occurrence probabilities

Similar to the preceding work by Lobzin and Pavlov (2002), the total number of hourly measurements studied is 20 532 879 which includes 69 443 G condition occurrences and 2 711 074 F1-layer occurrences. Our *Nm*F2 disturbance analysis includes only negative and positive ionospheric disturbances that have reference quiet days (see Sect. 3). A part

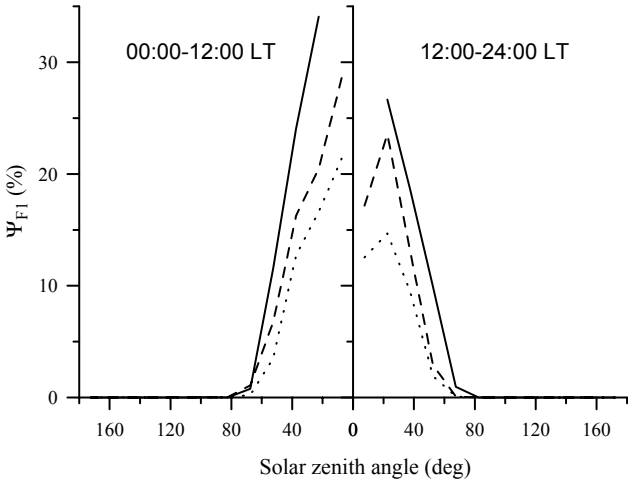

Fig. 1. The dependence of the F1-layer percentage occurrences on the solar zenith angle in latitude range 1 ($|\Phi| \leq 10°$) during the winter (solid lines), summer (dashed lines), and spring and autumn (dotted lines) months. The $0° - 180°$ solar zenith angle range includes the local time period from 00:00 LT to 12:00 LT (left panel) and from 12:00 LT to 24:00 LT (right panel).

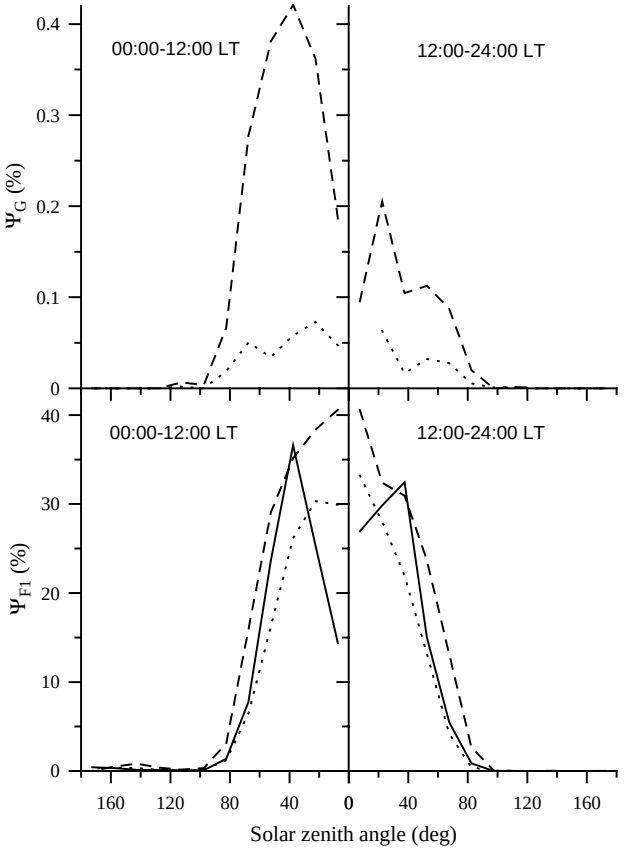

Fig. 2. The dependence of the F1-layer (two bottom panels), and G condition (two top panels) probability functions on the solar zenith angle in latitude range 2 ($10° < |\Phi| \leq 30°$) during the winter (solid lines), summer (dashed lines), and spring and autumn (dotted lines) months before midday from 00:00 LT to 12:00 LT (left panels), and after midday from 12:00 LT to 24:00 LT (right panels).

of the hourly *fo*f2 disturbance measurements has no reference quiet days, in agreement with the quiet day definition accepted in our paper, and these hourly *fo*f2 measurements are not analyzed.

Average values of $\Psi_{F1}(\chi)$ and $\Psi_G(\chi)$ are presented in Table 1. For each studied latitude range and season, the first number is determined as an average value, $< \Psi_{F1}(\chi) >_1$, of $\Psi_{F1}(\chi)$ or an average value, $< \Psi_G(\chi) >_1$, of $\Psi_G(\chi)$ for the first half of a day for $\chi \leq 90°$, while the second number is determined as an average value, $< \Psi_{F1}(\chi) >_2$, of $\Psi_{F1}(\chi)$ or an average value, $< \Psi_G(\chi) >_2$, of $\Psi_G(\chi)$ for the second half of a day for $\chi \leq 90°$. Table 1 shows that $< \Psi_{F1}(\chi) >_2$ is less than $< \Psi_{F1}(\chi) >_1$, except for latitude range 5 during the winter, spring, and autumn months. Our calculations show that $< \Psi_G(\chi) >_2$ is less than $< \Psi_G(\chi) >_1$ in latitude ranges 2–5 for all seasons, except for latitude range 3 in winter. For latitude range 3, $< \Psi_G(\chi) >_2$ is approximately equal to $< \Psi_G(\chi) >_1$ for all seasons.

The dependencies of the F1-layer percentage occurrences on the solar zenith angle in latitude range 1 are shown in Fig. 1 for the local time period from 00:00 LT to 12:00 LT (left panel) and from 12:00 LT to 24:00 LT (right panel). Figures 2–5 show the dependence of the F1-layer (bottom panels) and G condition (top panels) percentage occurrence on the solar zenith angle in latitude range 2 (Fig. 2), in latitude range 3 (Fig. 3), in latitude range 4 (Fig. 4), and in latitude range 5 (Fig. 5), during the winter (solid lines), summer (dashed lines), and spring and autumn (dotted lines) months. The left panels of Figs. 2–5 represent the F1-layer and G condition percentage occurrence from 00:00 LT to 12:00 LT, while the right panels of Figs. 2–5 give the F1-layer and G condition percentage occurrence from 12:00 LT to 24:00 LT. It should be noted that the calculated value of the G condition occurrence probability is negligible above the geomagnetic equatorial region (latitude range 1) during all seasons and in latitude range 2 in winter. Therefore, the $\Psi_G(\chi)$ dependencies are not discussed in this work for these cases.

Figures 2–5 show that the G condition is more likely to occur during the first half of a day than during the second half of a day in latitude ranges 2–5 during all seasons for the same value of the solar zenith angle, except for latitude range 3 in winter, when the G condition occurrence probability is approximately the same for the same solar zenith angle before and after 12:00 LT. The F1-layer occurrence probability is larger in the first half of a day in comparison with that in the second half of a day for the same value of the solar zenith angle within latitude range 1 for all seasons, while the F1-layer occurrence probability is approximately the same for the same solar zenith angle before and after 12:00 LT in latitude ranges 4 and 5.

It can be seen from Figs. 1–5 that the F1-layer and G condition are more commonly formed near midday than near post sunrise or pre-sunset, when the F-region is in the sunlight. These results are in agreement with the conclusions

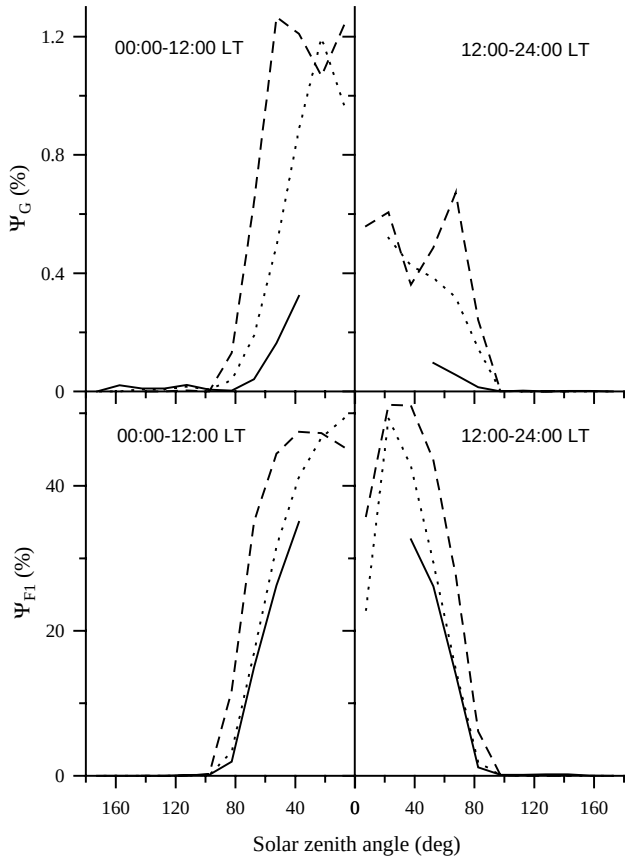

Fig. 3. The dependence of the F1-layer (bottom panels), and G condition (top panels) probability functions on the solar zenith angle in latitude range 3 ($30° < |\varphi| \leq 45°, 30° < |\Phi| \leq 45°$) during the winter (solid lines), summer (dashed lines), and spring and autumn (dotted lines) months before midday from 00:00 LT to 12:00 LT (left panels), and after midday from 12:00 LT to 24:00 LT (right panels).

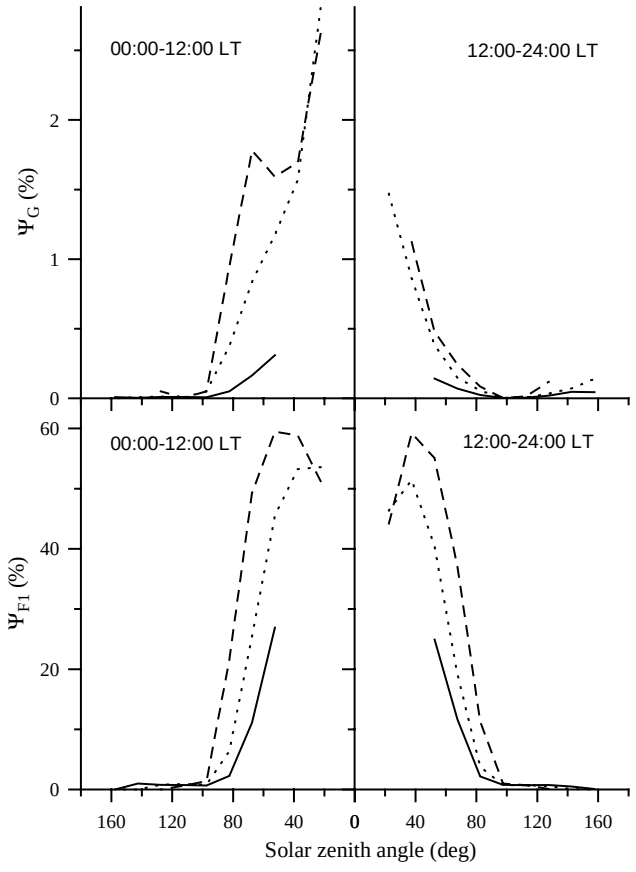

Fig. 4. The dependence of the F1-layer (bottom panels), and G condition (top panels) probability functions on the solar zenith angle in latitude range 4 ($45° < |\varphi| \leq 60°, 45° < |\Phi| \leq 60°$) during the winter (solid lines), summer (dashed lines), and spring and autumn (dotted lines) months before midday from 00:00 LT to 12:00 LT (left panels), and after midday from 12:00 LT to 24:00 LT (right panels).

of previous studies (for more details, see, for example, Ratcliffe, 1956, 1972; Yonezawa et. al., 1959; Polyakov et al., 1968) based on the theoretical studies and the limited data set. Figures 1–5 provide for the first time the quantitative measure of the probability variations with solar zenith angle changes. Figures 1–4 show that the maximum values of the F1-layer and G condition occurrence probabilities are located in the $0° - 45°$ solar zenith angle range in latitude ranges 1–4. The maximum values of the F1-layer and G condition occurrence probabilities are realized for the minimum value of χ close to noon in latitude range 5 (see Fig. 5). At the minimum solar zenith angle values (see Figs. 2–3), the number of observations is large enough for the identifiable oscillations in the probabilities at these solar zenith angles to be statistically significant. The physical reasons for the occurence of these oscillations are unclear.

The comparison in the values of $\Psi_{F1}(\chi)$ and $\Psi_G(\chi)$ between the five latitude regions described above shows the daytime tendency for a decrease in these probabilities at low latitudes and an increase in these probabilities at high latitudes for all seasons.

In the previous F1-layer and G condition studies (Ratcliffe, 1956, 1972; Polyakov et al., 1968; Shchepkin et al., 1984) based on the limited data set, it was demonstrated that the chance that the F1-layer and G condition will be formed is greater in summer than in winter. Lobzin and Pavlov (2002) have provided additional evidence of this phenomenon by calculating for the first time the diurnally average F1-layer and G condition probability variations with season. Comparison between solid (winter months), dashed (summer months), and dotted (spring and autumn months) lines in Figs. 2–5 gives a more detailed picture of the F1-layer and G condition seasonal probability behavior for the given solar zenith angle in each latitude ranges 1–5, thereby providing evidence that the chance that the daytime F1-layer and G condition will be formed is greater in summer than in winter. We have found for the first time that the F1-layer occurrence probability is greater in winter than in summer for all solar zenith angles above the geomagnetic equatorial region (see Fig. 1). It should also be noted that the F1-layer and G condition seasonal probabilities are lower during the spring and autumn months as compared with that during

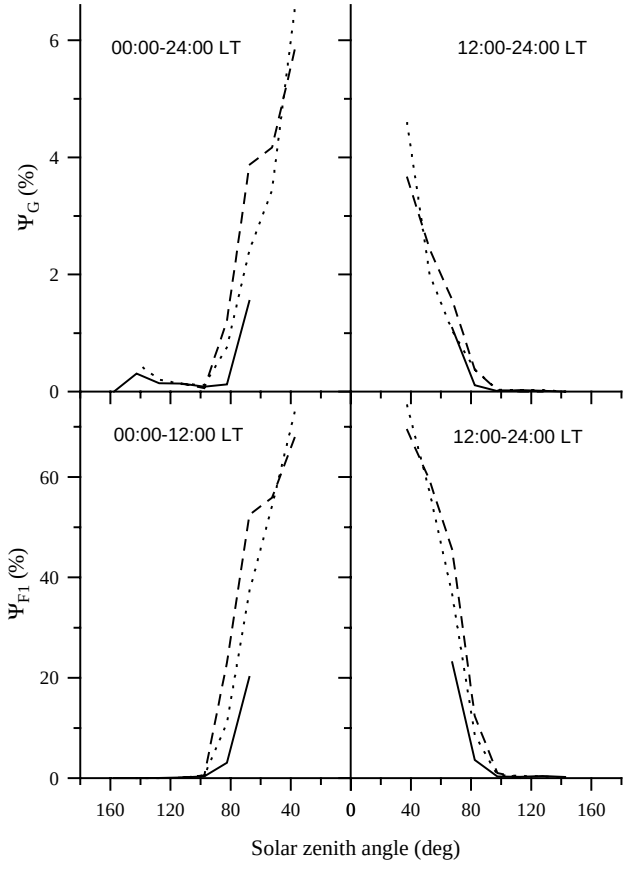

Fig. 5. The dependence of the F1-layer (bottom panels), and G condition (top panels) probability functions on the solar zenith angle in latitude range 5 ($60^\circ < |\Phi| \leq 90^\circ$) during the winter (solid lines), summer (dashed lines), and spring and autumn (dotted lines) months before midday from 00:00 LT to 12:00 LT (left panels), and after midday from 12:00 LT to 24:00 LT (right panels).

the summer months for most of the solar zenith angle range in latitude ranges 3–5 (compare dotted and dashed lines of Figs. 3–5).

Scotto et al. (1998) found that the probability of evaluating the occurrence of the F1-layer can be presented as

$$P_S(\Phi, \chi) = 100\,(1 - (\chi/90))^K \text{ for } \chi < 90^\circ,$$
$$\text{and } P_S(\Phi, \chi) = 0 \text{ for } \chi \leq 90^\circ, \quad (4)$$

where $K = 6.42182 - 0.00252479\Phi^2 + 4.02531 \times 10^{-7}\Phi^4$, and the unit of P_S is percent. The analysis of Scotto et al. (1998) was based on data acquired by the Ionospheric Digital Database of the National Geophysical Data Center, Boulder, Colorado, from 1969 to 1990. The value of $P_S(\Phi, \chi)$ approaches 100% for $\chi = 0^\circ$ and 0% for $\chi = 90^\circ$.

By comparing the dependence of the F1-layer occurrence probability on the solar zenith angle found in our work in each latitude range with $P_S(\Phi, \chi)$, we conclude that $P_S(\Phi, \chi)$ overestimates the real value of the F1-layer occurrence probability shown in Figs. 1–5. For example, 80% $\leq P_S(\Phi, \chi) \leq 100\%$ for $0^\circ \leq \chi \leq 52^\circ$ in the geomagnetic latitude range of $-45^\circ \leq \Phi \leq 45^\circ$, which includes latitude ranges 1–3 with the F1-layer occurrence probability shown in Figs. 1–3. It is also unclear why there are no seasonal differences in the dependence of P_S on χ. The details of deriving Eq. (4) are not presented in the short paper by Scotto et al. (1998), and we cannot give an explanation of the identifiable differences between our results and $P_S(\Phi, \chi)$.

4.2 *Nm*F2 normal, strong and very strong negative disturbance occurrence probabilities

Average values of all studied *Nm*F2 negative disturbance probabilities calculated in all latitude ranges and during all seasons are presented in Table 2. For each sort of *Nm*F2 negative disturbance, studied latitude range and season, the first number is determined as an average value, $< \Psi_{\delta 1 \leq \delta \leq \delta 0}(\chi) >_1$ of $\Psi_{\delta 1 \leq \delta \leq \delta 0}(\chi)$ for the first half of a day for $\chi \leq 90^\circ$, while the second number is determined as an average value, $< \Psi_{\delta 1 \leq \delta \leq \delta 0}(\chi) >_2$, of $\Psi_{\delta 1 \leq \delta \leq \delta 0}(\chi)$ for the second half of a day for $\chi \leq 90^\circ$. The third number is determined as an average value of $\Psi_{\delta 1 \leq \delta \leq \delta 0}(\chi)$ for the night-time period for $\chi > 90^\circ$. An average daytime value of any *Nm*F2 negative disturbance probability is calculated as a half-sum of the first and second numbers given in Table 2.

Table 2 shows that $< \Psi_{\delta 1 \leq \delta \leq \delta 0}(\chi) >_2$ is less than the $< \Psi_{\delta 1 \leq \delta \leq \delta 0}(\chi) >_1$ for the normal, strong or very strong *Nm*F2 negative disturbances in latitude ranges 3–5 for all seasons, except for the very strong *Nm*F2 negative disturbances in latitude ranges 3 in the winter and in latitude range 5 during winter, spring, and autumn months, when $< \Psi_{\delta \leq -0.5}(\chi) >_2$ is approximately equal to $< \Psi_{\delta \leq -0.5}(\chi) >_1$. In opposition to latitude ranges 3–5, $< \Psi_{\delta \leq -0.5}(\chi) >_1$ is less than $< \Psi_{\delta \leq -0.5}(\chi) >_2$ for the normal, strong, and very strong *Nm*F2 negative disturbances in latitude ranges 1 and 2 in winter, except for the very strong *Nm*F2 negative disturbances in latitude range 2 during all seasons and that in latitude range 1 during the summer and winter months. We found that $< \Psi_{\delta \leq -0.5}(\chi) >_1$ is approximately equal to $< \Psi_{\delta \leq -0.5}(\chi) >_2$ in latitude range 2 during all seasons.

Figures 6–10 show the dependence of the *Nm*F2 negative disturbance percentage occurrence on the solar zenith angle in latitude range 1 (Fig. 6), in latitude range 2 (Fig. 7), in latitude range 3 (Fig. 8), in latitude range 4 (Fig. 9), and in latitude range 5 (Fig. 10) during the winter (solid lines), summer (dashed lines), and spring and autumn (dotted lines) months for the weak (panels a), normal (panels b), strong (panels c), and very strong (panels d) *Nm*F2 negative disturbances. Left panels give the results for the local time period from 00:00 LT to 12:00 LT, while the right panels present the results of calculations from 12:00 LT to 24:00 LT. The first thing to note from Figs. 6–10 is that our results clearly capture the latitude dependence in the *Nm*F2 normal, strong and very strong negative disturbance probabilities, reproducing the general tendency for a decrease in these probabilities at low latitudes and an increase in probabilities at high latitudes, in agreement with previous conclusions of Lobzin and Pavlov (2002), who have calculated the diurnally and sea-

Table 2. Average values of weak, normal, strong, and very strong *Nm*F2 negative disturbance percentage occurrence in latitude ranges 1–5 during the winter, summer, and spring and autumn months for the first (first number) and second (second number) half of a day for $\chi \leq 90°$, and during the night-time period for $\chi > 90°$ (third number)

		Latitude range 1	Latitude range 2	Latitude range 3	Latitude range 4	Latitude range 5
Weak	Winter	31.3, 30.8, 21.0	28.4, 27.9, 20.9	32.7, 31.5, 25.2	32.1, 34.1, 24.4	26.3, 27.4, 18.0
	Summer	33.1, 28.3, 19.0	29.9, 28.0, 22.3	28.4, 30.9, 30.1	30.9, 36.6, 29.4	33.4, 36.4, 22.2
	Spring, autumn	30.3, 29.5, 20.6	29.8, 30.4, 22.0	31.0, 32.8, 28.3	27.6, 32.2, 25.6	28.7, 28.6, 17.4
Normal	Winter	10.7, 13.0, 18.7	15.5, 16.5, 21.1	12.9, 12.5, 21.6	23.7, 17.4, 25.2	36.1, 33.1, 22.3
	Summer	11.8, 17.8, 20.6	21.7, 23.7, 26.6	30.3, 27.2, 29.9	35.3, 27.2, 32.6	36.7, 33.8, 33.6
	Spring, autumn	9.3, 12.5, 17.7	15.7, 17.2, 22.6	23.0, 21.7, 22.4	35.2, 29.8, 28.2	38.3, 36.7, 25.0
Strong	Winter	0.1, 0.2, 4.8	1.4, 1.7, 5.5	0.8, 0.4, 2.9	3.7, 2.0, 5.7	9.5, 9.2, 9.3
	Summer	0.4, 0.6, 5.3	3.2, 3.9, 6.8	5.2, 3.3, 3.0	4.5, 1.7, 7.5	5.0, 3.2, 12.6
	Spring, autumn	0.2, 0.3, 3.8	1.6, 1.9, 6.0	4.0, 3.4, 2.9	7.9, 4.7,, 7.6	8.0, 7.5, 11.6
Very strong	Winter	0.02, 0.01, 0.9	0.1, 0.1, 0.7	0.1, 0.1, 0.2	0.3, 0.2, 0.6	1.1, 1.1, 2.5
	Summer	0.04, 0.03, 1.0	0.2, 0.1, 0.7	0.2, 0.1, 0.2	0.3, 0.1, 1.1	0.2, 0.1, 1.6
	Spring, autumn	0.02, 0.04, 0.8	0.2, 0.1, 0.9	0.3, 0.2, 0.3	0.5, 0.2, 1.2	0.5, 0.5, 3.3

son average dependencies of the *Nm*F2 negative disturbance probability functions on the geomagnetic latitude for $\delta < 0$, $\delta \leq -0.1$, $\delta \leq -0.3$, and $\delta \leq -0.5$.

Table 2 and Figs. 6 and 7 show that the *Nm*F2 normal, strong, and very strong negative disturbances are more frequent on average at night than by day in latitude ranges 1 and 2 for all seasons, reaching their maximum and minimum occurrence probability values at night and by day, respectively. This conclusion is also correct for all other studied latitude regions during the winter months (see Table 2 and solid lines in Figs. 8–10), except for the *Nm*F2 normal and strong negative disturbances in latitude range 5 (see Figs. 10b, c). Table 2 and the dashed and dotted lines in Figs. 9c, d and Figs. 10c, d show that the average night-time occurrence probability is larger than the average daytime occurrence probability for the strong and very strong negative disturbances in latitude ranges 4 and 5 during the summer, spring, and autumn months.

The Joule heating of the thermosphere can be viewed as the frictional heating produced in the thermosphere as the rapidly convecting ions collide with neutral molecules. Most of the Joule heating is deposited in the 115–150 km altitude region, although some extends to higher altitudes (Richmond and Lu, 2000). The geomagnetic storm Joule heating of the thermosphere is considerably more effective than the energy of the auroral electrons in affecting the thermospheric circulation and in the increase in the neutral temperature (Richmond and Lu, 2000). Joule heating from the dissipation of ionospheric currents raises the neutral temperature of the upper thermosphere, and the ion drag drives the high-velocity neutral winds during geomagnetic storms at high latitudes (Prölss, 1980, 1995; Fuller-Rowell et al., 1996, 2000). It leads to generation of a disturbed composition zone of the high-latitude neutral atmosphere, with an increase in heavier gases and a decrease in lighter gases, i.e. with an increase in $[N_2]$ and $[O_2]$ and in the $[N_2]/[O]$ and $[O_2]/[O]$ ratios. The wind surge propagates from aurora regions to low latitudes in both hemispheres. As a result, thermospheric altitude distributions of neutral species at middle and low latitudes are influenced by a global, large-scale wind circulation which is produced by a geomagnetic storm energy input at high latitudes (theoretical and observational studies of thermospheric composition responses to the transport of neutral species from auroral regions to middle latitudes during geomagnetic storms are reviewed by Prölss, 1980, 1995). The increase in the $[N_2]/[O]$ ratio maximises in a region that is roughly located in the vicinity of the auroral oval, and this $[N_2]/[O]$ increase intensifies and can expand to middle magnetic latitudes with the K_p increase (Brunelli and Namgaladze, 1988; Prölss, 1980, 1995; Zuzic et al., 1997; Buonsanto, 1999). The high-latitude geomagnetic storm upwelling brings air rich in the heavy species N2 and O2 to high altitudes, and the geomagnetic storm circulation carries this N_2 and O_2-rich air to mid-latitudes and lower latitudes. The geomagnetic storm downwelling leads to the opposite effect: air with low values of $[N_2]$ and $[O_2]$ is carried downward, reducing their concentrations at all altitudes (e.g. Fuller-Rowell et al., 1996; Field et al., 1998; Richmond and Lu, 2000). Thus, the values of $[N_2]$ and $[O_2]$, and the $[N_2]/[O]$ and the $[O_2]/[O]$ ratios are more enhanced at high latitudes than at middle latitudes, contributing to more *Nm*F2 decreases at high latitudes than at middle latitudes. The geomagnetic storm N_2 and O_2 number densities, and the $[N_2]/[O]$ and the $[O_2]/[O]$ ratios are depleted at low latitudes, causing *Nm*F2 increases at low latitudes. As a result, the daytime and night-time latitude trends in the probabilities of *Nm*F2 negative disturbances shown in Figs. 6–10 can arise from these latitude trends in $[N_2]$, $[O_2]$, $[N_2]/[O]$, and $[O_2]/[O]$.

As was described above, an additional enhanced equatorward wind arises during a geomagnetic storm, leading to

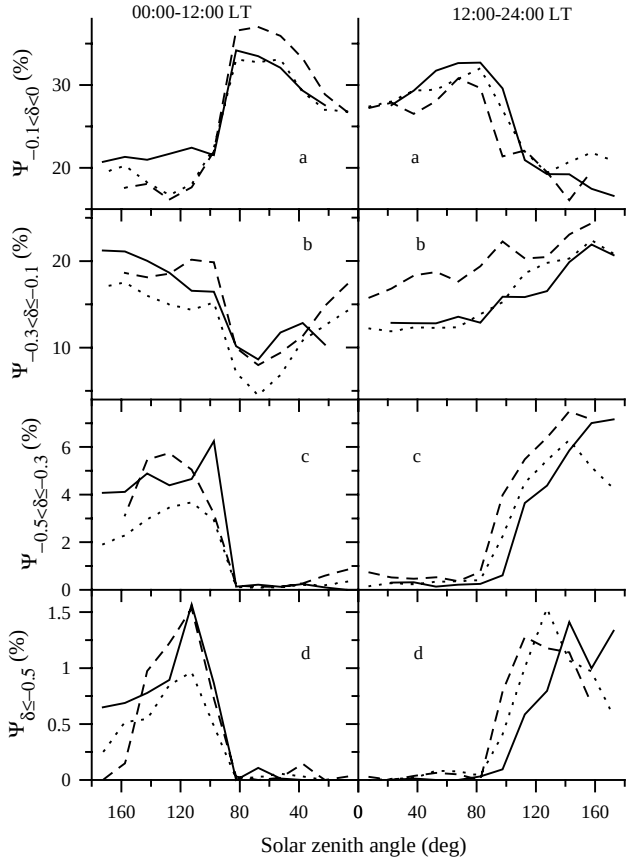

Fig. 6. The dependence of the *Nm*F2 negative disturbance probability functions on the solar zenith angle in latitude range 1 ($|\Phi| \leq 10°$) during the winter (solid lines), summer (dashed lines), and spring and autumn (dotted lines) months for the weak (panels a), normal (panels b), strong (panels c), and very strong (panels d) *Nm*F2 negative disturbances. The $0° - 180°$ solar zenith angle range includes the local time period from 00:00 LT to 12:00 LT (left panels) and from 12:00 LT to 24:00 LT (right panels).

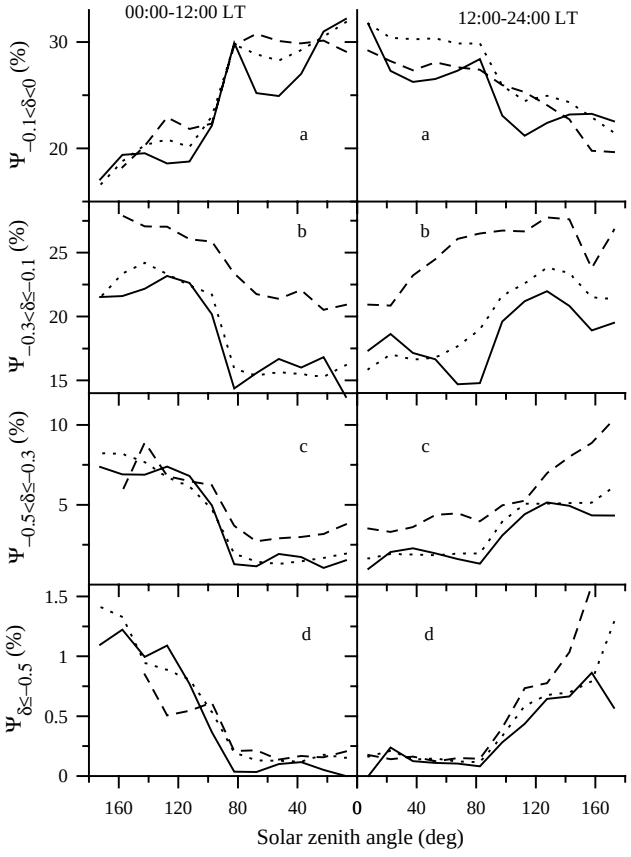

Fig. 7. The dependence of the *Nm*F2 negative disturbance probability functions on the solar zenith angle in latitude range 2 ($10° < |\Phi| \leq 30°$) during the winter (solid lines), summer (dashed lines), and spring and autumn (dotted lines) months for the weak (panels a), normal (panels b), strong (panels c), and very strong (panels d) *Nm*F2 negative disturbances. The $0° - 180°$ solar zenith angle range includes the local time period from 00:00 LT to 12:00 LT (left panels) and from 12:00 LT to 24:00 LT (right panels).

transport of neutral composition changes to lower latitudes. The resulting equatorward wind is stronger at night, because the additional geomagnetic storm equatorward wind is added to the quiet day-to-night circulation and because the additional wind is reinforced by antisunward ion drag due to magnetospheric convection $\boldsymbol{E} \times \boldsymbol{B}$ drifts (Straus and Schulz, 1976; Babcock and Evans, 1979). As a result, the neutral composition disturbance zone reaches more lower latitudes at night than by day, and the *Nm*F2 normal, strong and very strong negative disturbances tend to be more frequent on average at night than by day in latitude ranges 1 and 2 for all seasons (see Figs. 6 and 7). On the other hand, a rise in *hm*F2 to regions with a reduced loss rate of $O^+(^4S)$ ions due to equatorward winds produces an increase in *Nm*F2, while a drop in *hm*F2 due to poleward winds reduces *Nm*F2. This competition between a neutral composition disturbance causing *Nm*F2 negative storm effects and a rise in *hm*F2 causing *Nm*F2 positive storm effects determines the complicated dependence of the normal, strong and very strong *Nm*F2 negative disturbance percentage occurrences on the solar zenith angle (see Figs. 6–10).

We found that there is a difference between the dependence of the strong and very strong *Nm*F2 negative disturbance percentage occurrences on the solar zenith angle in latitude ranges 1 and 2 (see Figs. 6c, d and Figs. 7c, d). There are clear discriminated peaks in the probabilities of the strong and very strong *Nm*F2 disturbances before sunrise for all seasons in latitude range 1, while the strong and very strong *Nm*F2 negative disturbance occurrence probabilities are decreased (with some oscillations) with the decrease in the solar zenith angle in the post midnight night-time sector in latitude range 2. Our calculations show (see Figs. 9c, d and Figs. 10c, d) that the $\Psi_{-0.5<\delta\leq-0.3}(\chi)$ peak and the $\Psi_{\delta\leq-0.5}(\chi)$ peak in the post midnight night-time sector are accompanied by the $\Psi_{-0.5<\delta\leq-0.3}(\chi)$ peak and the $\Psi_{\delta\leq-0.5}(\chi)$ peak in the sunset-to-midnight sector in latitude ranges 4 and 5 during the winter, spring, and autumn months.

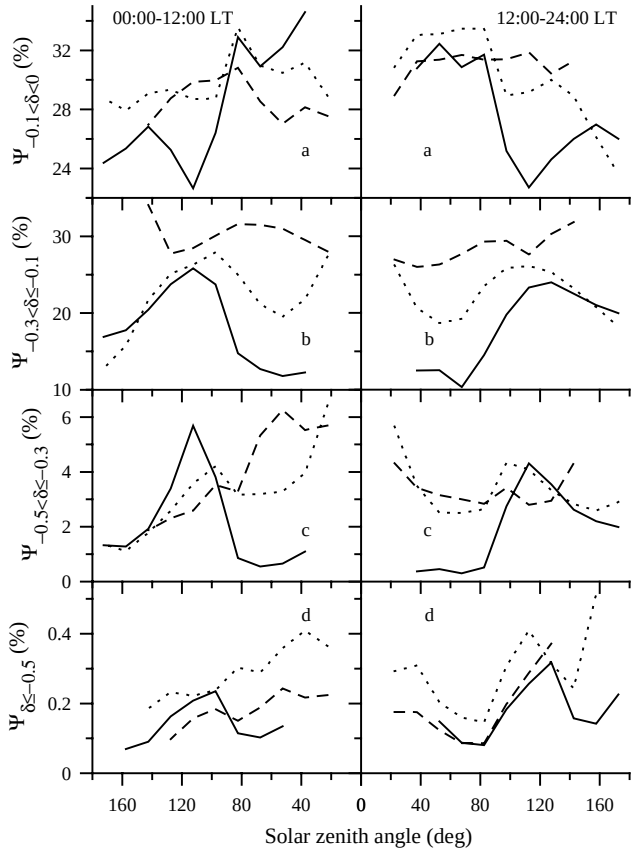

Fig. 8. The dependence of the *Nm*F2 negative disturbance probability functions on the solar zenith angle in latitude range 3 ($30° < |\varphi| \leq 45°, 30° < |\Phi| \leq 45°$) during the winter (solid lines), summer (dashed lines), and spring and autumn (dotted lines) months for the weak (panels a), normal (panels b), strong (panels c), and very strong (panels d) *Nm*F2 negative disturbances. The $0° - 180°$ solar zenith angle range includes the local time period from 00:00 LT to 12:00 LT (left panels) and from 12:00 LT to 24:00 LT (right panels).

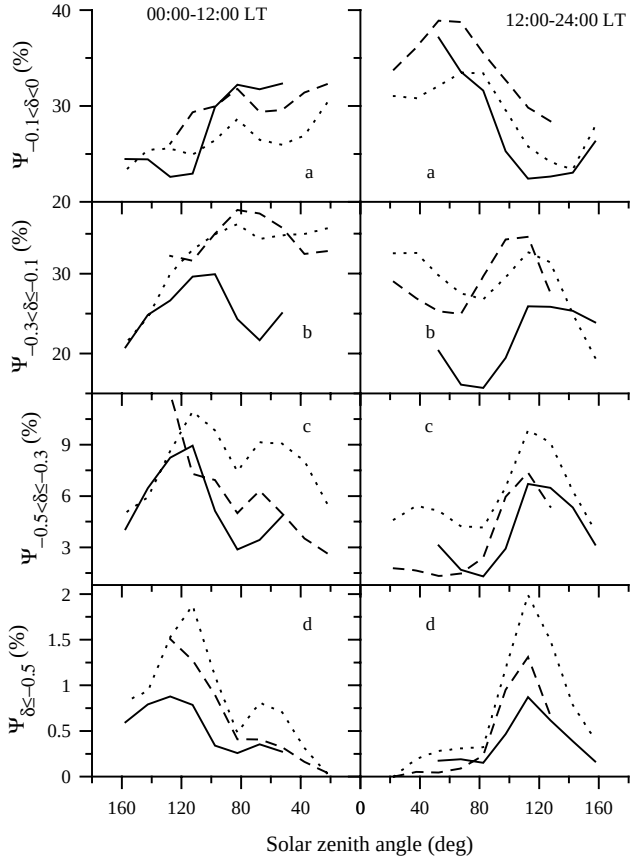

Fig. 9. The dependence of the *Nm*F2 negative disturbance probability functions on the solar zenith angle in latitude range 4 ($45° < |\varphi| \leq 60°, 45° < |\Phi| \leq 60°$) during the winter (solid lines), summer (dashed lines), and spring and autumn (dotted lines) months for the weak (panels a), normal (panels b), strong (panels c), and very strong (panels d) *Nm*F2 negative disturbances. The $0° - 180°$ solar zenith angle range includes the local time period from 00:00 LT to 12:00 LT (left panels) and from 12:00 LT to 24:00 LT (right panels).

4.3 *Nm*F2 weak negative disturbance occurrence probabilities

Average values of the weak *Nm*F2 negative disturbance probabilities calculated for all latitude ranges and seasons are presented in Table 2. For each studied latitude range and season, the first number is determined as an average value, $< \Psi_{-0.1<\delta<0}(\chi) >_1$, of $< \Psi_{-0.1<\delta<0}(\chi)$ for the first half of a day for $\chi \leq 90°$, while the second number is determined as an average value, $< \Psi_{-0.1<\delta<0}(\chi) >_2$, of $< \Psi_{-0.1<\delta<0}(\chi)$ for the second half of a day for $\chi \leq 90°$. The third number is determined as an average value of $\Psi_{-0.1<\delta<0}(\chi)$ for the night-time period for $\chi > 90°$. An average daytime value of the weak *Nm*F2 negative disturbance probability is calculated as a half-sum of the first and second numbers given in Table 2, shows that $< \Psi_{-0.1<\delta<0}(\chi) >_2$ is less than $< \Psi_{-0.1<\delta<0}(\chi) >_1$ in latitude ranges 3–5 for all seasons, except for latitude range 3 in winter and latitude range 5 for the spring and autumn months. In opposition to latitude ranges 3–5, where $< \Psi_{-0.1<\delta<0}(\chi) >_1$ is less than $< \Psi_{-0.1<\delta<0}(\chi) >_2$ in latitude ranges 1 and 2 for all seasons, except for latitude range 2 for spring and autumn months.

The top panels of Figs. 6–10 show that the occurrence probability of the *Nm*F2 weak negative disturbances reaches its maximum and minimum values during daytime and night-time conditions, respectively. It also follows from Table 2 that the average night-time value of this probability is less than that by day for all seasons in all latitude regions.

It should be noted that the F2-layer reaction to weak storms and to substorms is not easily directly observable, since weak effects are masked by ionization variations or by other variations that are not related to geomagnetic activity (hour-to-hour and day-to-day variability, etc.). The variations in the neutral atmosphere, the neutral winds, and the solar EUV flux can be reflected in the variability of *Nm*F2, and it is ascertained that night-time variability is larger than daytime variability of *Nm*F2 (Forbes et al., 2000). Published

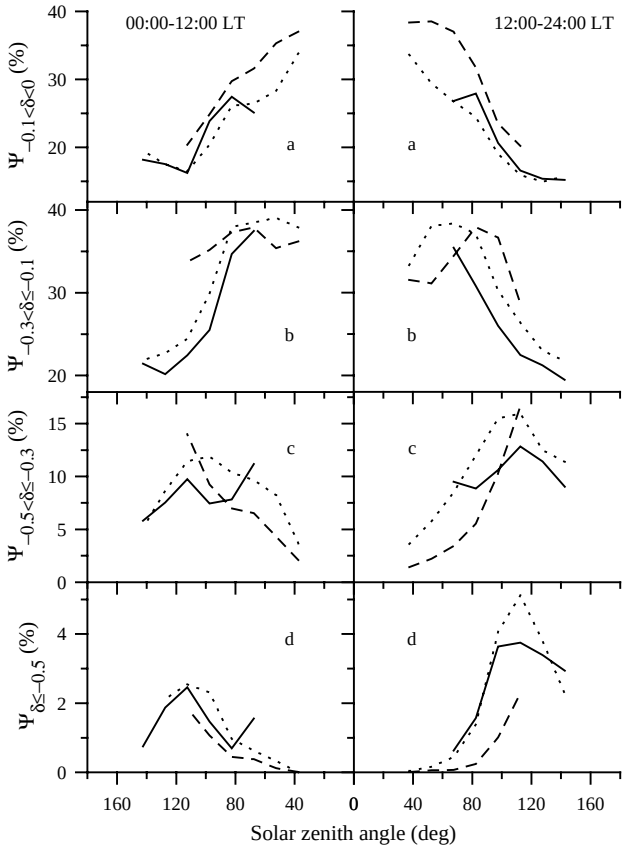

Fig. 10. The dependence of the *Nm*F2 negative disturbance probability functions on the solar zenith angle in latitude range 5 ($60° < |\Phi| \leq 90°$) during the winter (solid lines), summer (dashed lines), and spring and autumn (dotted lines) months for the weak (panels a), normal (panels b), strong (panels c), and very strong (panels d) *Nm*F2 negative disturbances. The $0° - 180°$ solar zenith angle range includes the local time period from 00:00 LT to 12:00 LT (left panels) and from 12:00 LT to 24:00 LT (right panels).

values of ionospheric electron content were used by Aravindakshan and Iyer (1993) to study its day-to-day variability at a number of stations extending from equatorial to mid-latitudes in Indian and American sectors for high and low solar activity years. The variability is larger at night than by day, highest in February and November and lowest in equinox months (Aravindakshan and Iyer, 1993). As a result, we conclude that the identifiable greater probability of the *Nm*F2 weak negative disturbances by day than at night (see the top panels of Figs. 6–10) is not related with a variability in the ionosphere.

In addition to the modified large-scale circulation of the neutral atmosphere, during geomagnetic disturbances, the spatial and temporal variations of high-latitude thermosphere heat sources excite large amplitude gravity waves, which produce travelling ionospheric disturbances in the F-region of the ionosphere (Millward et al., 1993; Hocke and Schlegel, 1996). Such gravity waves propagate from high to low latitudes considerably faster in the thermosphere than typical mid- and low-latitude winds resulting from storms (Rees, 1995; Hocke and Schlegel, 1996). The response of the mid-latitude ionosphere to this gravity waves propagation is observed by ionozonde stations and incoherent scatter radars in the raising or lowering of *hm*F2, often by several 10s of km, leading to a decrease or an increase in L and [O] at *hm*F2, i.e. leading to the increase or decrease in *Nm*F2, respectively (Rees, 1995; Hocke and Schlegel, 1996). The analysis of *fo*f2 measurements shows that night-time *fo*f2 decreases due to gravity wave propagation are not so significant as by day (Deminova et al., 1998). As a result, we conclude that the identifiable greater probability of the *Nm*F2 weak negative disturbances by day than at night, shown in the top panels of Figs. 6–10, can be explained if we suggest that *Nm*F2 weak negative disturbances are created by gravity wave propagation in the ionosphere.

4.4 Relationships between the F1-layer, *Nm*F2 negative disturbance, and G condition occurrence probability dependencies on χ

Figures 2–5 show that the daytime dependence of the F1-layer occurrence probability on the solar zenith angle is generally in phase with that for the G condition in latitude ranges 3–5 for all seasons, and in latitude range 2 during the spring, summer, and autumn months. However, we can conclude from Fig. 2 that this daytime coupling is less convincing in latitude range 2 during the winter months. The competition between the F1 and F2-layers for density dominance determines the G condition occurrence probability. Therefore, the occurrence probabilities of the weak, normal, strong, and very strong *Nm*F2 negative disturbances, in addition to the F1-layer occurrence probability, must be considered in addressing the causes of G condition solar zenith angle changes and in studying the possible relationships between the F1-layer and *Nm*F2 negative disturbance occurrences. The G condition in the geomagnetically disturbed ionosphere is associated mainly with a significant negative ionospheric storm in *Nm*F2 (Lobzin and Pavlov, 2002). Thus, the found F1-layer occurrence probability dependence on the solar zenith angle (see the low panels of Figs. 2–5) and the identifiable solar zenith angle trends in strong and very strong negative disturbance probabilities shown in panels (c) and (d) of Figs. 7–10, are the trends involved in the formation of the G condition solar zenith angle tendencies shown in the top panels of Figs. 2–5.

A decrease in the solar zenith angle leads to decreases in the daytime values of strong and very strong negative disturbance occurrence probabilities in latitude ranges 4 and 5 for the spring, summer, and autumn months (dashed and dotted lines in panels (c) and (d) of Figs. 9 and 10). The daytime probabilities $\Psi_{-0.3\leq\delta<-0.1}(\chi)$, and $\Psi_{\delta\leq-0.5}(\chi)$ of the *Nm*F2 negative disturbance occurrence do not show discriminated trends in an increase or a decrease with the solar zenith angle decrease in latitude range 2 for all seasons (panels (c) and (d) of Fig. 7), and in all the studied latitude regions for the winter months (solid lines in panels (c) and (d) of Figs. 6–10). This

means that that the dependence of the F1-layer occurrence probability on χ is the main source which contributes to the daytime $\Psi_G(\chi)$ trend in the all studied latitude regions for the winter months, in latitude range 2 for all the seasons, and in latitude ranges 4 and 5 for spring, summer, and autumn months.

The results presented in panels (c) and (d) of Fig. 7 show that the occurrence probabilities of the strong and very strong negative disturbances in latitude range 3 is increased with some oscillations if the solar zenith angle is increased. On the other hand, if we do not take into consideration the $0^\circ - 15^\circ$ solar zenith angle range during the summer, spring, and autumn months, then we can conclude that the F1-layer occurrence probability is decreased in latitude range 3 if the solar zenith angle is increased (see Fig. 3). This means that the solar zenith angle trend in the G condition occurrence probability arises in the main from the solar zenith angle trend in the F1-layer occurrence probability of this latitude region. The solar zenith angle trend in the probabilities of strong and very strong *Nm*F2 negative disturbances counteracts the solar zenith angle trend in the probability of the G condition occurrence shown in the upper panels b and c of Fig. 3.

5 Conclusions

The primary goal of the present work is to calculate the dependencies of the *Nm*F2 negative disturbance, F1-layer and G condition occurrence probabilities on the solar zenith angle during the summer, winter, spring and autumn months in latitude range 1 ($|\Phi| \leq 10^\circ$), in latitude range 2 ($10^\circ < |\Phi| \leq 30^\circ$), in latitude range 3 (both $30^\circ < |\varphi| \leq 45^\circ$ and $30^\circ < |\Phi| \leq 45^\circ$), in latitude range 4 (both $45^\circ < |\varphi| \leq 60^\circ$ and $45^\circ < |\Phi| \leq 60^\circ$), and in latitude range 5 ($60^\circ < |\Phi| \leq 90^\circ$), using experimental data acquired by the Ionospheric Digital Database of the National Geophysical Data Center, Boulder, Colorado, from 1957 to 1990. The G condition cannot exist in the ionosphere if there is no F1-layer. During ionospheric disturbances, the *Nm*F2 decrease leads to the increase in the G condition occurrence probability if the F1-layer exists. The relationships between the G condition, F1-layer, and *Nm*F2 negative disturbance occurrence probabilities are also studied in this paper.

5.1 F1-Layer and the G condition

Our calculations show that the G condition is more likely to occur during the first half of a day than during the second half of a day, in latitude ranges 2–5 during all seasons for the same value of the solar zenith angle, except for latitude range 3 in winter, when the G condition occurrence probability is approximately the same for the same solar zenith angle before and after 12:00 LT for $\chi \leq 90^\circ$.

We found that the average value for the second half of a day of the F1-layer occurrence probability is less than that for the first half of a day, except for latitude range 5 during the winter, spring, and autumn months. The F1-layer occurrence probability is larger in the first half of a day in comparison with that in the second half of a day for the same value of the solar zenith angle in latitude range 1 for all seasons, while the F1-layer occurrence probability is approximately the same for the same solar zenith angle before and after noon in latitude ranges 4 and 5 for $\chi \leq 90^\circ$.

We found that the F1-layer and G condition are more commonly formed near midday than close to post sunrise or presunset, when the F-region is in the sunlight. The maximum values of the F1-layer and G condition occurrence probabilities are found to be in the $0^\circ - 45^\circ$ solar zenith angle range in latitude ranges 1–4. The maximum values of the F1-layer and G condition occurrence probabilities are realized for the minimum value of χ close to noon in latitude range 5.

The comparison in the values of the F1-layer and G condition occurrence probabilities between all studied latitude ranges shows the daytime tendency for a decrease in these probabilities at low geomagnetic latitudes and an increase in these probabilities at high geomagnetic latitudes for all seasons. The identifiable detailed picture of the F1-layer and G condition seasonal probability behavior at the given solar zenith angle in latitude ranges 2–5 provides evidence that the chance that the daytime F1-layer and G condition will be formed is greater in summer than in winter. We have found for the first time that the F1-layer occurrence probability is greater in winter than in summer for all solar zenith angles in latitude range 1. The identifiable F1-layer and G condition seasonal probabilities are lower during the spring and autumn months as compared with that during the summer months for most of the solar zenith angle range in latitude ranges 3–5.

5.2 Negative *Nm*F2 disturbances

The magnitudes of the studied *Nm*F2 weak, normal, strong and very strong negative disturbances and their extension to lower latitudes are controlled by a number of parameters, including the strength of the magnetospheric storm or substorm, the season, the latitude, and the solar zenith angle. Our results clearly capture the geomagnetic latitude dependence in the *Nm*F2 normal, strong, and very strong negative disturbance probabilities, reproducing the general tendency for a decrease in these probabilities at low latitudes and an increase in the probabilities at high latitudes. We found that the *Nm*F2 normal, strong, and very strong negative disturbances are more frequent on average at night than by day, in latitude ranges 1 and 2 for all seasons, reaching their maximum and minimum occurrence probability values at night and by day, respectively. This conclusion is also correct for all other studied latitude regions during the winter months, except for the *Nm*F2 normal and strong negative disturbances in latitude range 5. The calculated average night-time occurrence probability is larger than the average daytime occurrence probability for the strong and very strong negative disturbances in latitude ranges 4 and 5 during the summer, spring, and autumn months.

It is proved that the average value for the second half of a day of the *Nm*F2 negative disturbance probability is less than that for the first half of a day for the normal, strong, and very strong *Nm*F2 negative disturbances in latitude ranges 3–5 for all seasons, except for the very strong *Nm*F2 negative disturbances in latitude ranges 3 in winter and in latitude range 5 during the winter, spring, and autumn months, when the average value of the very strong *Nm*F2 negative disturbances for $\chi \leq 90^\circ$ is approximately the same before and after 12:00 LT. In opposition to latitude ranges 3–5, the average value for the first half of a day of the *Nm*F2 negative disturbance probability is less than that for the second half of a day for the normal, strong, and very strong *Nm*F2 negative disturbances in latitude ranges 1 and 2 in winter, except for the very strong *Nm*F2 negative disturbances in latitude range 2 during all seasons and that in latitude range 1 during the summer and winter months. The average value of the very strong *Nm*F2 negative disturbances for $\chi \leq 90^\circ$ is approximately the same before and after 12:00 LT in latitude range 2.

We found that there is a difference between the dependence of the strong and very strong *Nm*F2 negative disturbance percentage occurrences on the solar zenith angle in latitude ranges 1 and 2. There is a clear, discriminated peak in the probability of the strong or very strong *Nm*F2 disturbance before sunrise for all seasons in latitude range 1. The strong and very strong *Nm*F2 negative disturbance occurrence probabilities are decreased (with some oscillations) with the decrease in the solar zenith angle in the post midnight sector in latitude range 2. Our calculations show that the strong and very strong *Nm*F2 negative disturbance occurrence probability peaks in the post midnight night-time sector are accompanied by the peaks in these probabilities in the sunset-to-midnight sector in latitude ranges 4 and 5 during the winter, spring, and autumn months.

It is proved that that the average value for the second half of a day of the weak *Nm*F2 negative disturbance probability is less than that for the first half of a day in latitude ranges 3–5 for all seasons, except for latitude range 3 in winter and latitude range 5 for the spring and autumn months. In opposition to latitude ranges 3–5, the average value for the first half of a day of the weak *Nm*F2 negative disturbance probability is less than that for the second half of a day in latitude ranges 1 and 2 for all seasons, except for latitude range 2 for the spring and autumn months.

The calculated occurrence probability of the *Nm*F2 weak negative disturbances reaches its maximum and minimum values during daytime and night-time conditions, respectively, and the average night-time value of this probability is less than that by day for all seasons in all latitude regions. It is proved that an ionosphere variability that is not related to geomagnetic activity is not the cause of the *Nm*F2 weak negative disturbance probability variations. We have concluded that the identifiable greater probability of the *Nm*F2 weak negative disturbances by day than at night can be explained if we suggest that *Nm*F2 weak negative disturbances are created by gravity wave propagation in the ionosphere.

5.3 Relationships between the G condition, F1-layer, and *Nm*F2 negative disturbance occurrence probabilities

The competition between the F1- and F2-layers for density dominance determines the G condition occurrence probability. We found that the daytime dependence of the F1-layer occurrence probability on the solar zenith angle is generally in phase with that for the G condition in latitude ranges 3–5 for all seasons, and in latitude range 2 during the spring, summer, and autumn months, but this daytime coupling is less convincing in latitude range 1 during the winter months. On the other hand, the G condition in the geomagnetically disturbed ionosphere is associated mainly with a significant negative ionospheric storm in *Nm*F2. Thus, the identifiable F1-layer occurrence probability dependence on the solar zenith angle and the identifiable solar zenith angle trends in strong and very strong negative disturbance probabilities are the trends involved in the formation of the G condition solar zenith angle trends. Our calculations show that the main source which contributes to the daytime dependence of the G condition occurrence probability on the solar zenith angle in the all studied latitude regions for the winter months, in latitude range 2 for all seasons, and in latitude ranges 4 and 5 for the spring, summer, and autumn months, is the dependence of the F1-layer occurrence probability on the solar zenith angle. The solar zenith angle trend in the probability of the G condition occurrence in latitude range 3 arises in the main from the solar zenith angle trend in the F1-layer occurrence probability. The solar zenith angle trend in the probabilities of strong and very strong *Nm*F2 negative disturbances counteracts the identifiable solar zenith angle trend in the probability of the G condition occurrence.

Acknowledgements. The research described in this publication was supported by grant 99-05-65231 from the Russian Foundation for Basic Research. The authors would like to thank referees for their comments on the paper, which have assisted in improving the final version.

Topical Editor M. Lester thanks two referees for their help in evaluating this paper.

References

Abdu, M. A.: Outstanding problems in the equatorial ionospherethermosphere electrodynamics relevant to spread F, J. Atmos. Sol. Terr. Phys., 63, 869–884, 2001.

Aravindakshan, P. and Iyer, K. N.: Day-to-day variability in ionospheric electron content, J. Atmos. Terr. Phys., 55, 1565–1573, 1993.

Babcock, R. R., Jr. and Evans, J. V.: Seasonal and solar cycle variations in the thermospheric circulation observed over Millstone Hill, J. Geophys. Res., 84, 7348–7352, 1979.

Banks, P. M., Schunk, R. W., and Raitt, W. J.: NO^+ and O^+ in the high latitude F-region, Geophys. Res. Lett, 1, 239–242, 1974.

Buonsanto, M. J.: Observed and calculated F2 peak heights and derived meridional winds at mid-latitudes over a full solar cycle, J. Atmos. Terr. Phys., 52, 223–240, 1990.

Buonsanto, M. J.: Ionospheric storms – a review, Space Science Reviews, 88, 563–601, 1999.

Brunelli, B. E. and Namgaladze, A. A.: Physics of the ionosphere (in Russian), Nauka, Moscow, 1988.

Deminova, G. F., Shashunkina, V. M., and Goncharova, E. E.: A global empirical model of effects of large-scale internal gravity waves in the night-time ionosphere, J. Atmos. Sol. Terr. Phys., 60, 227–245, 1998.

DuCharme, E. D. and Petrie, L. E.: A method for predicting the F1-layer critical frequency based on the Zürich smoothed sunspot number, Radio Sci., 8, 837–839, 1973.

Fejer, B. G.: The electrodynamics of the low latitude ionosphere: recent results and future challenges, J. Atmos. Terr. Phys., 59, 1465–1482, 1997.

Field, P. R., Rishbeth, H., Moffett, R. J., Idenden, D. W., Fuller-Rowell, T. G., Millward, G. H., and Aylward, A. D.: Modelling composition changes in F-layer storms, J. Atmosph. Terr. Phys., 60, 523–543, 1998.

Forbes, J. M., Palo, S. E., and Zhang, X.: Variability of the ionosphere, J. Atmos. Terr. Phys., 62, 685–693, 2000.

Fukao, S., Oliver, W. L., Onishi, Y., Takami, T., Sato, T., Tsuda, T., Yamamoto, M., and Kato, S.: F-region seasonal behavior as measured by the MU radar, J. Atmos. Terr. Phys., 53, 599–618, 1991.

Fuller-Rowell, T. J., Codrescu, M. V., Moett, R. J., and Quegan, S.: On the seasonal response of the thermosphere and ionosphere to geomagnetic storms, J. Geophys. Res., 101, 2343–2353, 1996.

Fuller-Rowell, T. J., Codrescu, M. C., and Wilkinson, P.: Quantitative modeling of the ionospheric response to geomagnetic activity, Ann. Geophysicae, 18, 766–781, 2000.

Häggström, I. and Collis, P. N.: Ion composition changes during F-region density depletions in the presence of electric fields at auroral latitudes, J. Atmos. Terr. Phys., 52, 519–529, 1990.

Hedin, A. E.: MSIS-86 thermospheric model, J. Geophys. Res., 92, 4649–4662, 1987.

Hocke, K. and Schlegel, K.: A review of atmospheric gravity waves and travelling ionospheric disturbances: 1982–1995, Ann. Geophysicae, 14, 917–940, 1996.

King, G. A. M.: The ionospheric F-region during a storm, Planet. Space Sci., 9, 95-100, 1962.

Krinberg, I. A. and Tashchilin, A. V.: Refilling of geomagnetic force tubes with a thermal plasma after magnetic disturbance, Ann. Geophysicae, 38, 25–32, 1982.

Krinberg, I. A. and Tashchilin, A. V.: Ionosphere and plasmasphere, Nauka, Moscow, 1984 (in Russian).

Lobzin, V. V. and Pavlov, A. V.: G condition in the F2 region peak electron density: a statistical study, Ann. Geophysicae, 20, 523–537, 2002.

Millward, G. H., Moffett, R. J., Quegan, S., and Fuller-Rowell, R. G.: Effects of atmospheric gravity wave on the mid-latitude ionospheric F layer, J. Geophys. Res., 98, 19173–19179, 1993.

Norton, R. B.: The middle-latitude F-region during some severe ionospheric storms, Proc. IEEE, 57, 1147–1149, 1969.

Oliver, W. L.: Neutral and ion composition changes in the F-region over Millstone Hill during the equinox transition study, J. Geophys. Res., 95, 4129–4134, 1990.

Pavlov, A. V.: The role of vibrationally excited oxygen and nitrogen in the ionosphere during the undisturbed and geomagnetic storm period of 6–12 April 1990, Ann. Geophysicae, 16, 589–601, 1998.

Pavlov, A. V. and Buonsanto, M. J.: Anomalous electron density events in the quiet summer ionosphere at solar minimum over Millstone Hill, Ann. Geophysicae, 16, 460–469, 1998.

Pavlov, A. V., Buonsanto, M. J., Schlesier, A. C., and Richards, P. G.: Comparison of models and data at Millstone Hill during the 5–11 June 1991 storm, J. Atmosph. Terr. Phys., 61, 263–279, 1999.

Pavlov, A. V. and Foster, J. C.: Model/data comparison of F-region ionospheric perturbation over Millstone Hill during the severe geomagnetic storm of 15–16 July 2000, J. Geophys. Res., 105, 29 051–29 070, 2001.

Polyakov, I. A., Shchepkin, L. A., Kazimirovsky, E. S., and Kokourov, V. D.: Ionospheric processes (in Russian), Nauka, Novosibirsk, 1968.

Prölss, G. W.: Magnetic storm associated perturbations of the upper atmosphere: Recent results obtained by satellite-borne gas analyzers, Rev. Geophys. Space Phys., 18, 183–202, 1980.

Prölss, G. W.: Ionospheric F-region storms, In Handbook of Atmospheric Electrodynamic, ed. by H. Volland, 2, 195–248. CRC Press, Boca Raton, FL, 1995.

Ratcliffe, J. A.: The formation of the ionospheric layers F-1 and F-2, J. Atmosph. Terr. Phys., 8, 260–269, 1956.

Ratcliffe, J. A.: An introduction to the ionosphere and magnetosphere, Cambridge, University Press, 1972.

Rees, M. H.: Physics and chemistry of the upper atmosphere, Cambridge and New York, Cambridge University Press, 1989.

Rees, D.: Observations and modelling of ionospheric and thermospheric disturbances during major geomagnetic storms: A review, J. Atmosph. Sol. Terr. Phys., 57, 1433–1457, 1995.

Richmond, A. D. and Lu, G.: Upper-atmospheric effects of magnetic storms: a brief tutorial, J. Atmosph. Sol. Terr. Phys., 62, 1115–1127, 2000.

Rishbeth, H.: The equatorial F-layer: progress and puzzles, Ann. Geophysicae, 18, 730–739, 2000.

Rishbeth, H. and Garriot, O.: Introduction to ionospheric physics, New York, Academic Press, 1969.

Rishbeth, H. and Muller-Wodarg, I. C. F.: Vertical circulation and thermospheric composition: a modelling study, Ann. Geophysicae, 17, 794–805, 1999.

Rishbeth, H., Muller-Wodarg, I. C. F., Zou, L., Fuller-Rowell, T. J., Millward, G. H., Moffett, R. J., Idenden, D. W., and Aylward, A. D.: Annual and semiannual variations in the ionospheric F2-layer: II. Physical discussion, Ann. Geophysicae, 18, 945–956, 2000.

Schlesier, A. C. and Buonsanto, M. J.: Observations and modeling of the 10–12 April 1997 ionospheric storm at Millstone Hill, Geophys. Res. Lett., 26, 2359–2362, 1999.

Scotto, C., de Gonzalez, M. M., Radicella, S. M., and Zolesi, B.: On the prediction of F1 ledge occurrence and critical frequency, Advances in Space Research, 20, 9, 1773–1775, 1997.

Scotto, C., Radicella, S. M., and Zolesi, B.: An improved probability function to predict the F_1 layer occurrence and L condition, Radio Science, 33, 1763–1766, 1998.

Shchepkin, L. A., Vasiliev, K. N., Vinitskii, A. V., Grishkevich, L. V., Datsko, E. P., Kushnarenko, G. P., Moskaliuk, N. V., and Shulgina, V. I.: Seasonal variations of F1-layer parameters in a solar-maximum period (in Russian), Geomagnetism and Aeronomy, 34, 35–39, 1984.

Schunk, R. W., Raitt, W. J., and Banks, P. M.: Effects of electric fields on the daytime high-latitude E- and F-regions, J. Geophys. Res., 80, 3121–3130, 1975.

Sterling, D. L., Hanson, W. B., and Woodman, R. F.: Synthesis of data obtained at Jicamarca, Peru, during the 11 September 1969, eclipse, Radio Sci., 7, 279–289, 1972.

Straus, J. M. and Schulz, M.: Magnetospheric convection and upper atmospheric dynamics, J. Geophys. Res., 81, 5822–5832, 1976.

URSI handbook of ionogram interpretation and reduction, ed. by W. R. Piggott and K. Rawer, National Oceanic and Atmospheric Administration, Boulder, CO, 1978.

Wrenn, G. L., Rodger, A. S., and Rishbeth, H.: Geomagnetic storms in antarctic F-region. I. Diurnal and seasonal patterns for main phase effects, J. Atmosph. Terr. Phys., 49, 901–913, 1987.

Yonezawa, T., Takashi, H., and Arima, Y.: A theoretical consideration of the electron and ion density distribution in the lower portion of the F-region, J. Radio Res. Lab., 6, 21–46, 1959.

Zuzic, M., Scherliess, L., and Prölss, G. W.: Latitudinal structure of thermospheric composition perturbations, J. Atmosph. Terr. Phys., 59, 711–724, 1997.